Available online at www.sciencedirect.com
SCIENCE DIRECT®
PERGAMON
Geothermics 33 (2004) 457–476
GEOTHERMICS
www.elsevier.com/locate/geothermics

Numerical modeling of transient Basin and Range extensional geothermal systems

Jason R. McKenna*, David D. Blackwell

Department of Geological Sciences, Southern Methodist University, 3225 Daniel Street, Dallas, TX 75275, USA

Received 1 July 2003; accepted 2 October 2003

Available online 21 February 2004

Abstract

A suite of models utilizing a simplified structural framework with a range of bulk rock permeabilities were developed to analyze the transient behavior of Basin and Range extensional geothermal systems, and particularly, the evolution of the system temperature with time. Each model consists of two mountain ranges (∼1 km relief from the valley floor) separated by a thick sequence (about 4 km) of clastic sediments derived from the adjacent ranges, and a highly permeable, high-angle fault that functions as a conduit for subsurface fluids. This geometry is typical of Basin and Range extensional systems. We characterize the reservoir by utilizing several parameters, including temperature along the producing fault and the predicted surface heat flow. Time scales are on the order of 100 kyear for development of maximum reservoir temperatures. However, if not sealed, significant geothermal systems can exist on a steady-state basis. The models show some features seen in Dixie Valley, Naveda, and explain observed relationships that young faults are frequently associated with extensional geothermal systems.

Keywords: Extensional geothermal systems; Heat flow; Flow modeling; Basin and Range; Dixie Valley; USA

1. Introduction

Active geothermal systems, in which subsurface temperatures are sometimes in excess of 200 °C, and even 250 °C by 2–3 km depth, are associated with Quaternary normal faulting in the Basin and Range (Caskey et al., 2000). These systems are non-magmatic in origin, based on the helium isotope ratios in the hot water (Kennedy et al., 2000). Meteoric water enters

* Corresponding author. Tel.: +1-214-768-4140; fax: +1-214-768-2701.
E-mail address: jmckenna@mail.smu.edu (J.R. McKenna).

0375-6505/$30.00 © 2004 CNR. Published by Elsevier Ltd. All rights reserved.
doi:10.1016/j.geothermics.2003.10.001

via the range top or valley fill, warms during deep circulation, and ascends along the nearest, highest permeable pathway, usually an active range-bounding fault. One such Basin and Range geothermal system located in Dixie Valley, Nevada, is unusually hot: temperatures in excess of 280 °C have been encountered by 3 km depth (Blackwell et al., 2000).

Our objective in this study is to determine under what conditions a reservoir temperature near 280 °C is generated and, if possible, sustained. We characterize the reservoir by utilizing several parameters, including temperature along the producing fault, and the predicted surface heat flow. Fig. 1 is a shaded relief map of Dixie Valley, Nevada, and the adjacent region. Several hot springs and fumaroles are located within the valley, indicating high subsurface temperatures. Drilling indicates high temperatures (>190 °C) at 2.5–3.0 km depth along a strike length of at least 20 km along the west side of the valley (from the producing field to Dixie Meadows hot springs). Benoit (1999) and Blackwell et al. (1999, 2002) review and demonstrate structural models of the Dixie Valley geothermal system.

The geometry of the models we present is similar to the natural geometry of extensional geothermal systems. There are two mountain ranges in our models (∼1 km relief from the valley floor), separated by a valley filled with a thick sequence (about 4 km in our models) of clastic sediments derived from the adjacent ranges. There is a relatively permeable, high-angle fault (65°) that functions as a conduit for subsurface fluids at one of the valley/range contacts.

A previous modeling study to characterize the flow regime in these types of systems (Wisian, 2000), utilizing TOUGH2 (Pruess et al., 1999), concentrated on exploring the parameter space of steady-state numerical models with upflow along a permeable fault. The temperature distributions and energy transfer characteristics of these models were summarized in that paper. In this paper we describe the transient behavior of similar numerical models to illustrate the temporal complexity inherent in these systems, and as a potential explanation for reconciling higher observed reservoir temperatures than predicted by steady-state models.

2. Steady-state results

2.1. Model geometry

The two-dimensional geometry utilized in the numerical modeling is illustrated in Fig. 2a. The modeling parameters specific to each numbered domain are listed in Table 1. Note that the valley fill incorporates anisotropic permeability to more accurately mimic the hydrologic properties in the valley in accord with observations. The cell size away from the fault zone is 230 m × 200 m, whereas immediately adjacent to the fault, the cell size is halved (130 m × 100 m) to provide sufficient resolution of both the thermal and flow regime near the fault (Fig. 2b). The total number of elements is 7471.

The models we show were developed utilizing PetraSim by Thunderhead Engineering Consultants. Unless stated otherwise, all the models developed in this study utilize surface temperature and pressure boundary conditions of 20 °C, and 1×10^5 Pa, respectively. Additionally, a basal heat flow of 90 mW m^{-2} directed into the model (chosen so that the model accurately represents the high heat flow in the Basin and Range Province) is specified for

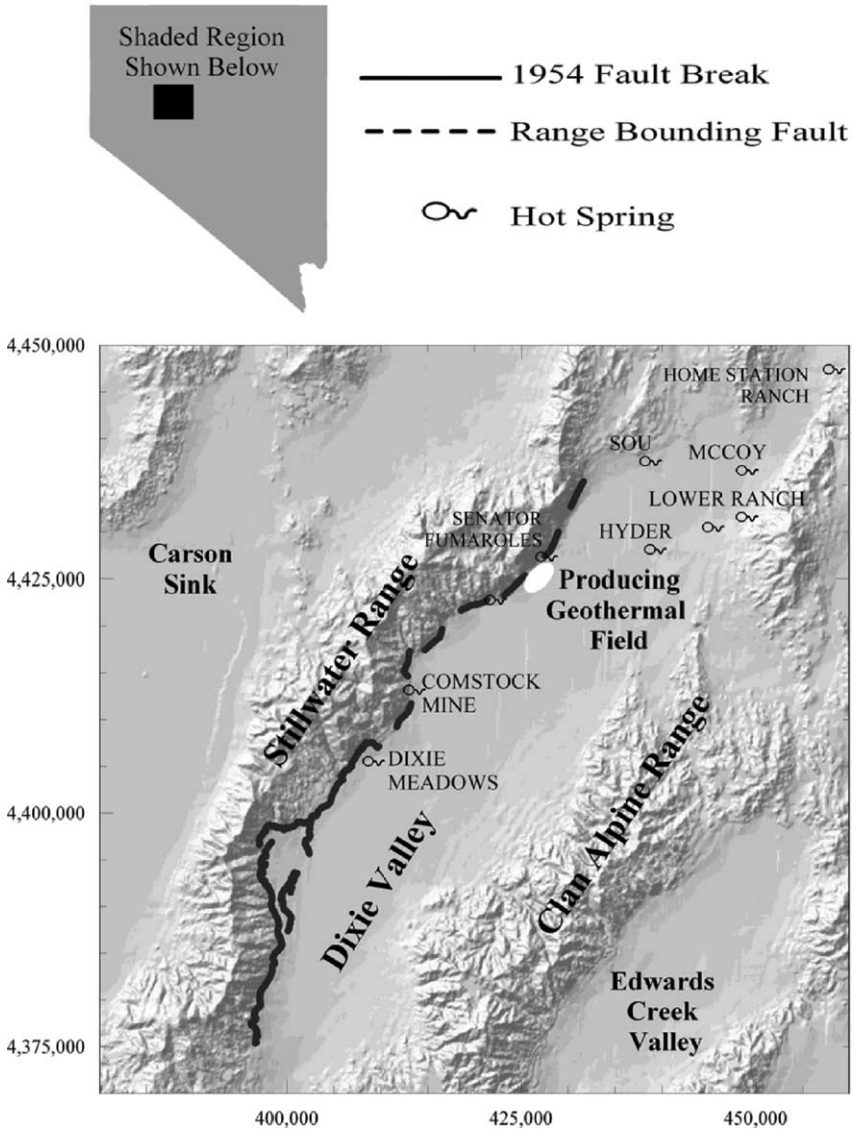

Fig. 1. Dixie Valley, Nevada. All subsequent numerical models attempt to model the “active geothermal area”.

the bottommost row of cells. Because the emphasis of our modeling is regional geothermal systems, we neglect the unsaturated zone in our modeling and require all elements to be fully saturated. Hence, we do not impose a radiative heat flow boundary condition on the surface of the model. The constraints on the mass flux estimates obtained from our models are discussed in a later section.

We utilize a modified version of the equation-of-state for pure water (EOS1) for TOUGH2 that allows for super-critical conditions in pure water (EOS1sc; Brikowski, 2001). Both

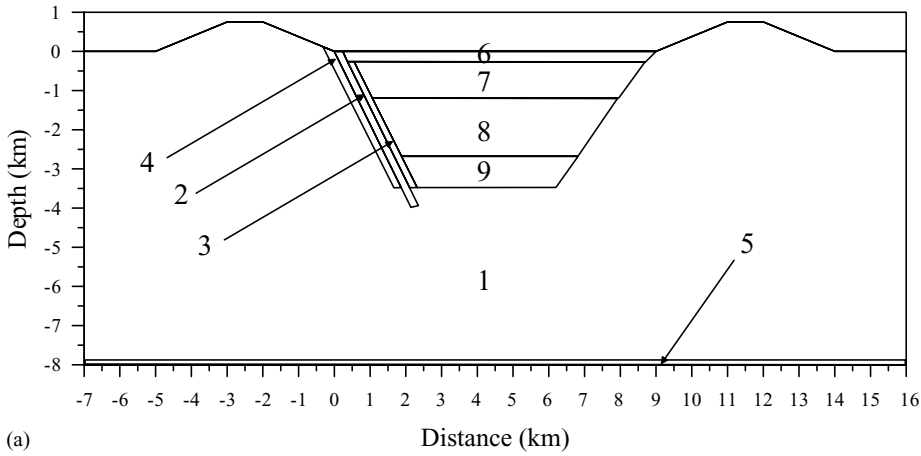

(a)

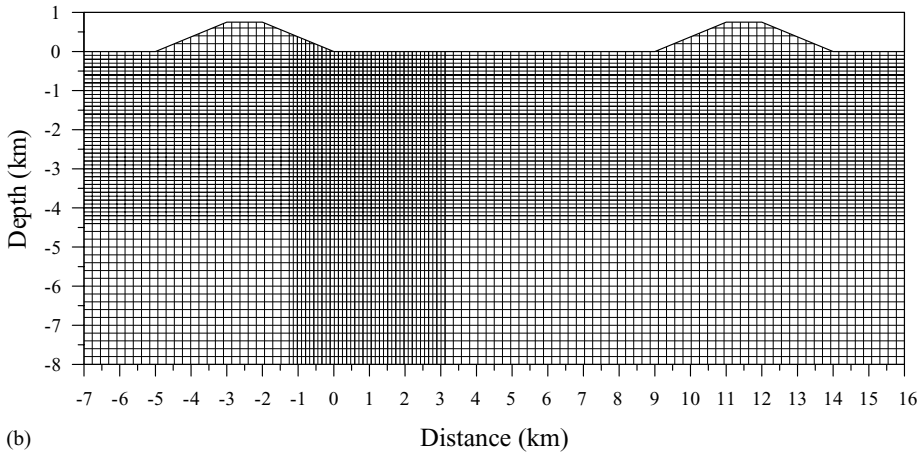

(b)

Fig. 2. (a) Model geometry. The domain number in the above figure corresponds with the domain number appearing in Table 1. (b) Model grid. The model consists of 7471 elements.

the EOS1 and EOS1sc modules yield almost identical results; however, because even non-magmatic geothermal systems are often near the critical point of pure water by 6–9 km depth, the latter module provides more realistic characterization of reservoir pressure–temperature conditions. Also, to facilitate direct comparison with future models with higher temperatures, we use the super-critical equation-of-state module.

2.2. Thermal and flow regime

The “normal” thermal/flow regime in Basin and Range settings remains poorly constrained. The background heat flow of the entire region is significantly elevated with respect to adjacent tectonic areas (e.g., Lachenbruch and Sass, 1978; Blackwell, 1983; Blackwell et al., 1991), but whether or not some regions beneath the ranges are naturally convecting

Table 1
TOUGH2 modeling parameters

Domain	Material	Porosity	Wet thermal conductivity ($Wm^{-1}\,K^{-1}$)	Horizontal permeability (m^2)	Vertical permeability (m^2)
1	Bulk rock	1.0E−01	2.50	Variable	Variable
2	Fault	1.0E−01	2.50	1.0E−14	1.0E−14
3	Fault (valley-side)	1.0E−01	1.25	1.0E−18	1.0E−18
4	Fault (range-side)	1.0E−01	2.50	1.0E−18	1.0E−18
5	Bottom	1.0E−05	2.50	1.0E−20	1.0E−20
6	Valley fill 1	1.0E−01	1.25	1.0E−15	1.0E−16
7	Valley fill 2	1.0E−01	1.25	1.0E−15	1.0E−16
8	Valley fill 3	1.0E−01	1.25	1.0E−15	1.0E−16
9	Valley fill 4	1.0E−01	1.25	1.0E−15	1.0E−16

A constant density and heat capacity of $2650\,kg\,m^{-3}$, and $1000\,J\,kg^{-1}\,K^{-1}$, respectively, were utilized in the modeling. The bulk rock permeability is varied in each model. A basal heat flow of $90\,mW\,m^{-2}$, surface temperature of 20 °C, and surface pressure of 1.01×10^5 Pa were specified as boundary conditions. The low value for the thermal conductivity is based on laboratory measurements obtained from cuttings up to 2.5 km depth. The low-permeability domains flanking the fault zone are utilized to represent probable fault-sealing.

remains unknown. Many Basin and Range geothermal systems are believed to initiate or become more vigorous as the range-bounding fault permeability abruptly increases during/after an earthquake (Parry et al., 1991). However, it is unclear whether the best initial pressure–temperature conditions for numerical modeling are an initially conductive or convective thermal/flow regime. To help address this uncertainty we discuss models that utilize both cases as initial conditions.

Fig. 3a shows the steady-state temperature and velocity distribution obtained after a simulation time of 32 Myear (hereafter referred to as steady-state), utilizing a bulk rock permeability of $1 \times 10^{-20}\,m^2$ (i.e., domain 1, see Fig. 2, see the more extensive discussion in Wisian, 2000). At such a low permeability, almost all the fluid velocities are extremely low (with the exception of the range tops where fluid enters the system), and the only observed thermal effect is a modest increase in temperature between the ranges (domains 6–9 in Fig. 2) caused by the low thermal conductivity valley fill. Both the linearity of the temperature along the fault as a function of depth (Fig. 4; see below) and the lack of anomalously high predicted surface heat flow at the fault/range contact (Fig. 5) illustrate that the model is essentially conductive. The model described above attempts to model a situation in which the host rock is essentially impermeable, whereas the valley fill and fault itself remain highly permeable. For simplicity we assume that the entire volume of the basement rock is impermeable. Fig. 3b and c is equivalent to the model shown in Fig. 3a, except that the bulk rock (domain 1), fault (domain 2), range-side fault (domain 4) and valley-side fault (domain 3) permeabilities were set at either $1 \times 10^{-16}\,m^2$ (Fig. 3b), or $5 \times 10^{-16}\,m^2$ (Fig. 3c) to simulate an actively convecting porous system prior to faulting, and development of the focused geothermal system. The steady-state simulations obtained from the models shown in Fig. 3 are utilized as the initial conditions for all subsequent models discussed here. More likely situations in which the bulk rock permeability decreases as depth increases (exponentially perhaps, see Ingebritsen, 1999), or the bulk permeability is randomly distributed, will be investigated in subsequent modeling.

We restrict the analysis in the rest of the paper to two values for the bulk rock permeability, 1×10^{-16} and $5 \times 10^{-16}\,m^2$, for two reasons. First, at bulk rock permeabilities $> 5 \times 10^{-16}\,m^2$, models do not attain steady-state prior to 100 Myear because they continue to cool and thus are unrealistic regional solutions. Second, at permeabilities lower than $1 \times 10^{-16}\,m^2$ models are essentially conductive: a model utilizing a bulk rock permeability of $1 \times 10^{-17}\,m^2$ generates fault temperatures that are $<2\,^{\circ}C$ different from the conductive model (i.e., a bulk rock permeability of $1 \times 10^{-20}\,m^2$, see Fig. 4 and also Wisian, 2000).

The steady-state results for bulk rock permeabilities of 1×10^{-16} and $5 \times 10^{-16}\,m^2$ utilizing the conductive initial conditions (see Fig. 3a) are shown in Figs. 6 and 7, respectively.

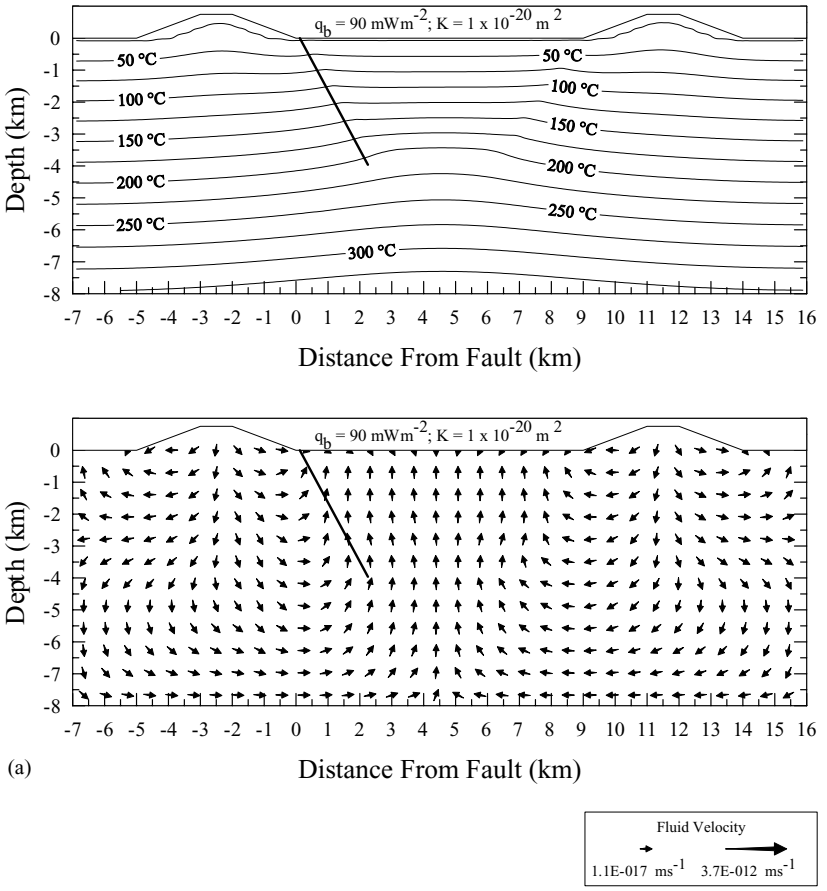

Fig. 3. (a) Steady-state thermal and flow regime obtained utilizing a bulk rock permeability of $1 \times 10^{-20}\,m^2$, and a basal heat flow of $90\,mW\,m^{-2}$. The permeable fault is shown as a heavy line. The thermal regime is essentially conductive. (b) Steady-state thermal and flow regime obtained utilizing a bulk rock permeability of $1 \times 10^{-16}\,m^2$ (domain 1) and a basal heat flow of $90\,mW\,m^{-2}$. In addition, the permeability of the fault (domain 2), range-side fault (domain 4), and valley-side fault (domain 3) were set to $1 \times 10^{-16}\,m^2$. (c) Identical to (b), except a permeability of $5 \times 10^{-16}\,m^2$ was utilized for domains 1,2,3 and 4.

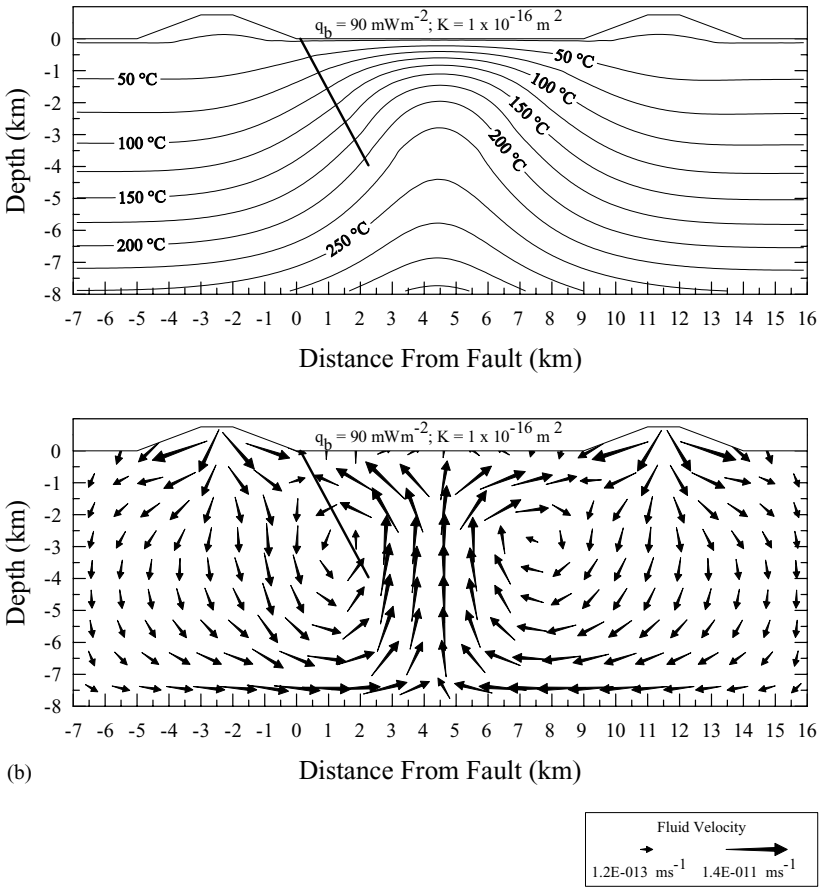

Fig. 3. (*Continued*)

Simulations obtained utilizing the convective initial conditions (Fig. 3b and c) are not shown because, at steady-state, the thermal and flow regimes for these models are identical to the results shown in Figs. 6 and 7. In both cases the simulations depict recharge in the ranges, whereas discharge occurs at the fault/valley fill contact. Because the fault serves as a conduit for the upflow of fluids, temperatures along the fault are at least 125 °C hotter than at the other side of the valley fill-range contact (Figs. 6 and 7).

Other than the qualitative similarities noted above, the thermal and flow regimes between the two permeabilities are quite different. The higher permeability case has significantly more fluid flow up the fault, partly because the greater permeability contrast between the anisotropic valley fill and bulk rock delivers more recharge from the adjacent ranges into the valley-fill sequence, and partly because the ∼4 km diameter secondary convection cells that have developed beneath the ranges help deliver more fluid to the fault inlet area. Hence, the flow field for the higher permeability case (5×10^{-16} m^2) is about a factor of 2 faster than for the lower permeability case (1×10^{-16} m^2). It is noted that a correspondingly

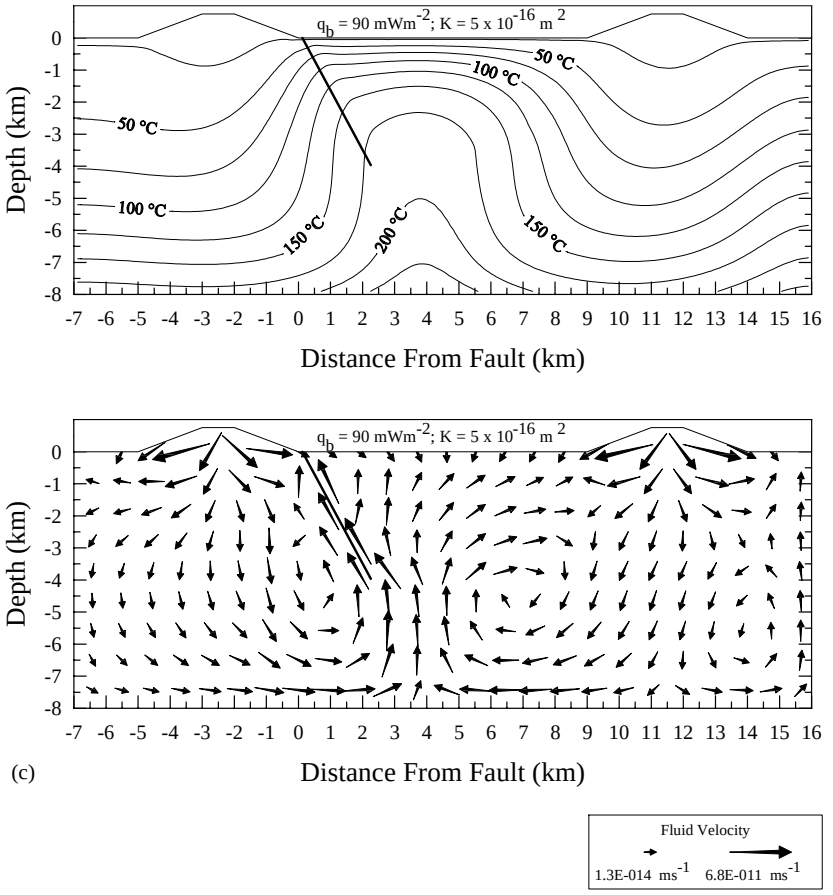

Fig. 3. (*Continued*).

greater recharge rate in the ranges is predicted to account for the large amount of fluid discharging at the fault/valley fill contact. Additionally, the lower permeability case (Fig. 6) has developed a convection cell wholly within the valley-fill sequence, and consequently receives less fluid from deeper sources. The models presented here predict a maximum steady-state discharge at the fault/valley contact of about 17,000 Lyear^{-1} (1×10^{-16} m^2 bulk rock permeability case) and about 45,000 Lyear^{-1} (5×10^{-16} m^2 bulk rock permeability case). We estimated the discharge in the Dixie Valley geothermal system at about 31,600 Lyear^{-1} by examining the heat loss from both the temperature data (Blackwell et al., 2000) and spring discharge within the Dixie Valley area. Given the uncertainty in our models and natural mass flows, the prediction of similar volumetric flow rates is encouraging.

In summary, the less vigorous flow regime for the lower bulk rock permeability model lacks the deeper, secondary convection observed for the higher bulk rock permeability model, probably because the flow is focused along the model boundaries.

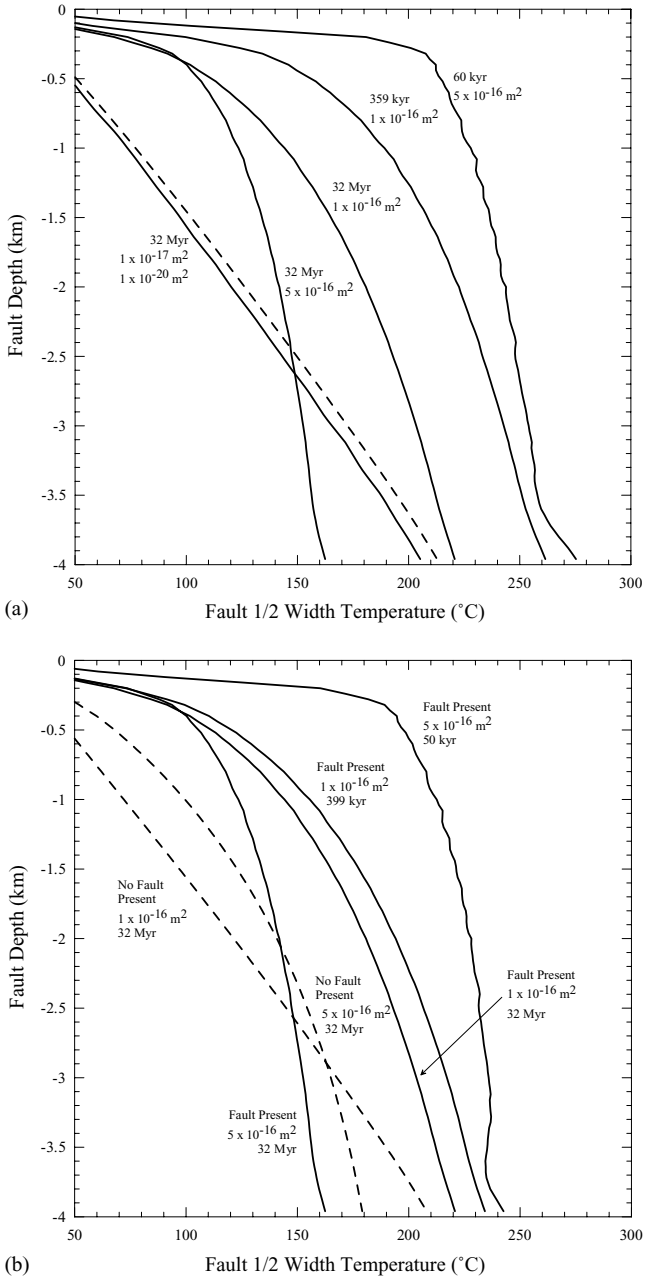

Fig. 4. (a) Predicted fault temperature for several bulk rock permeabilities and simulation times utilizing the conductive initial conditions shown in Fig. 3a. Dashed line corresponds to the 1×10^{-17} m^2 simulation. (b) Predicted fault temperature for several bulk rock permeabilities and simulation times utilizing the naturally convecting initial conditions shown in Fig. 3b and c.

Future models will expand the dimensions of the model to determine whether the lack of secondary convection beneath the ranges for lower permeability bulk rock is a meaningful result, or is simply a case of the model boundaries imposing the observed flow regime.

2.3. Surface heat flow

The steady-state predicted surface heat flow for the conductive initial condition models (i.e., models that utilize a bulk rock permeability of $1 \times 10^{-20}\,m^2$ at 32 Myear as initial conditions) and convective initial condition models (i.e., models that use bulk rock

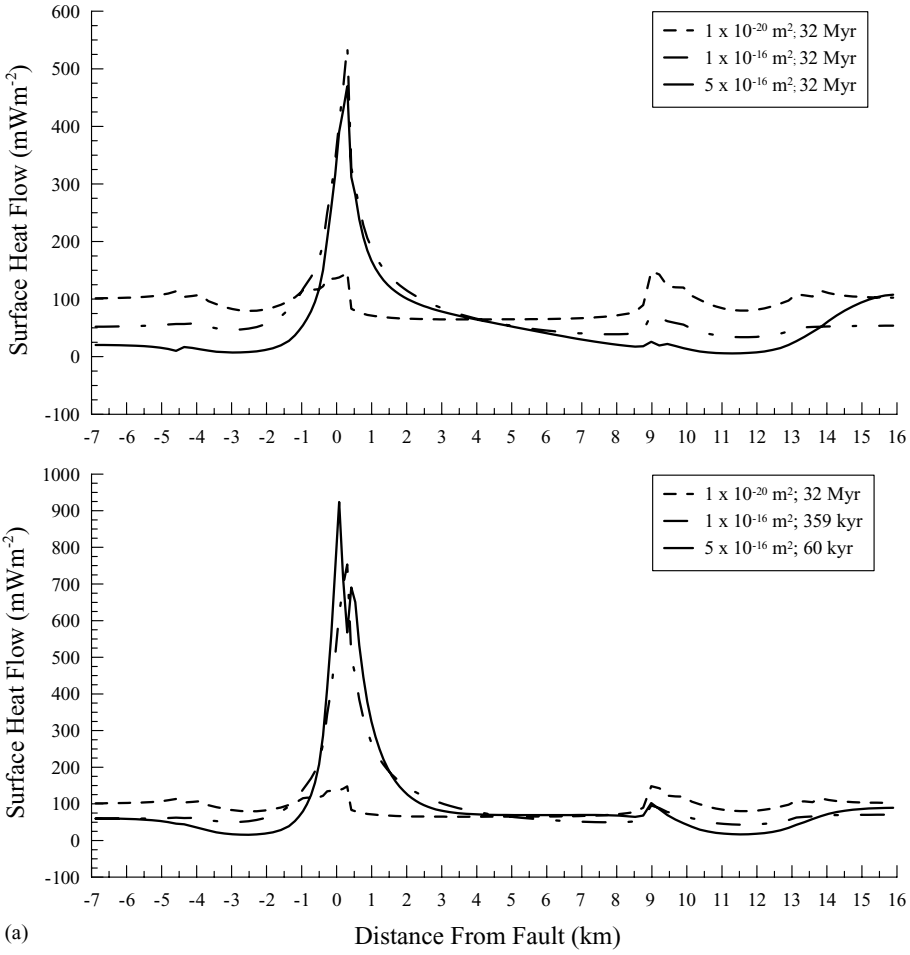

Fig. 5. (a) Predicted surface heat flow at 0 km depth for several bulk rock permeabilities and simulation times utilizing a conductive thermal regime as the initial condition. (b) Predicted surface heat flow at 0 km depth for several bulk rock permeabilities and simulation times utilizing a naturally convective medium as the initial condition.

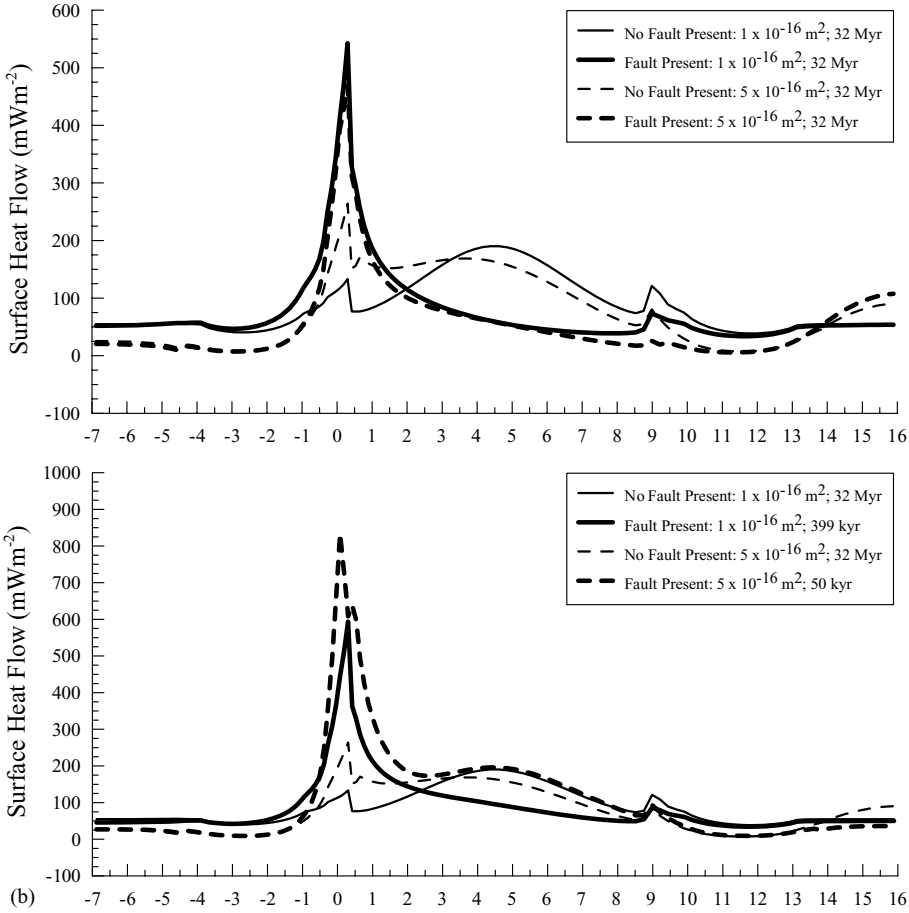

Fig. 5. (*Continued*).

permeabilities of 5×10^{-16} and 1×10^{-16} m^2 without a permeable fault at 32 Myear as initial conditions) are illustrated in Figs. 5a and b, respectively. In the case of the former, the initial heat flow distribution is approximately equal to the basal heat flow, although the overall shape of the curve is complicated by heat refraction effects from the dipping fault/valley fill contact. These models show a large (>450 mW m^{-2}) heat flow anomaly centered on the fault/valley fill contact. Additionally, the 1×10^{-16} m^2 model predicts a heat flow anomaly about 100 mW m^{-2} greater than the 5×10^{-16} m^2 bulk rock permeability model because the fluid recharge rate is higher in the ranges. For the convective models without a fault, the initial heat flow distribution shows a broad heat flow anomaly that is almost double the basal heat input, centered over (1×10^{-16} m^2 bulk rock permeability model), and nearer the left edge of the valley fill (5×10^{-16} m^2 bulk rock permeability model). At steady-state flow, these models are identical to the models with conductive initial conditions discussed previously.

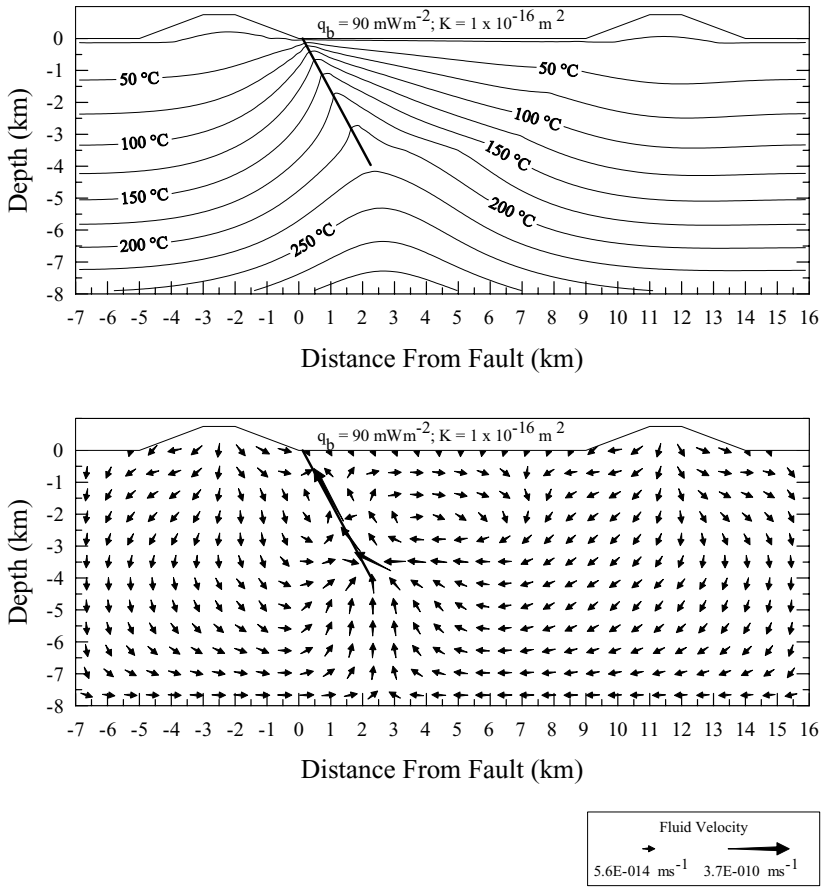

Fig. 6. Steady-state thermal and flow regime obtained utilizing a bulk rock permeability of 1×10^{-16} m^2, and a basal heat flow of 90 mW m^{-2}.

2.4. Fault temperature

The fault temperatures for the steady-state thermal regimes modeled in Figs. 6 and 7 are shown in Fig. 4a and b, along with the fault temperature–depth curves obtained from the three different initial condition scenarios shown in Fig. 3. In each case, the temperature is extracted along the fault (the solid line dipping at 65° in each thermal cross-section, see Figs. 3, 6 and 7) and plotted as a function of vertical depth. The maximum steady-state fault temperature is about 220 °C for the lower bulk rock permeability model and about 160 °C for the higher bulk rock permeability model. These temperatures are significantly lower than the ∼280 °C temperatures measured via precision temperature logs in Dixie Valley, and in the case of the higher bulk rock permeability model, extremely low (about 120 °C lower). The shape of the temperature–depth curves offers one possible explanation.

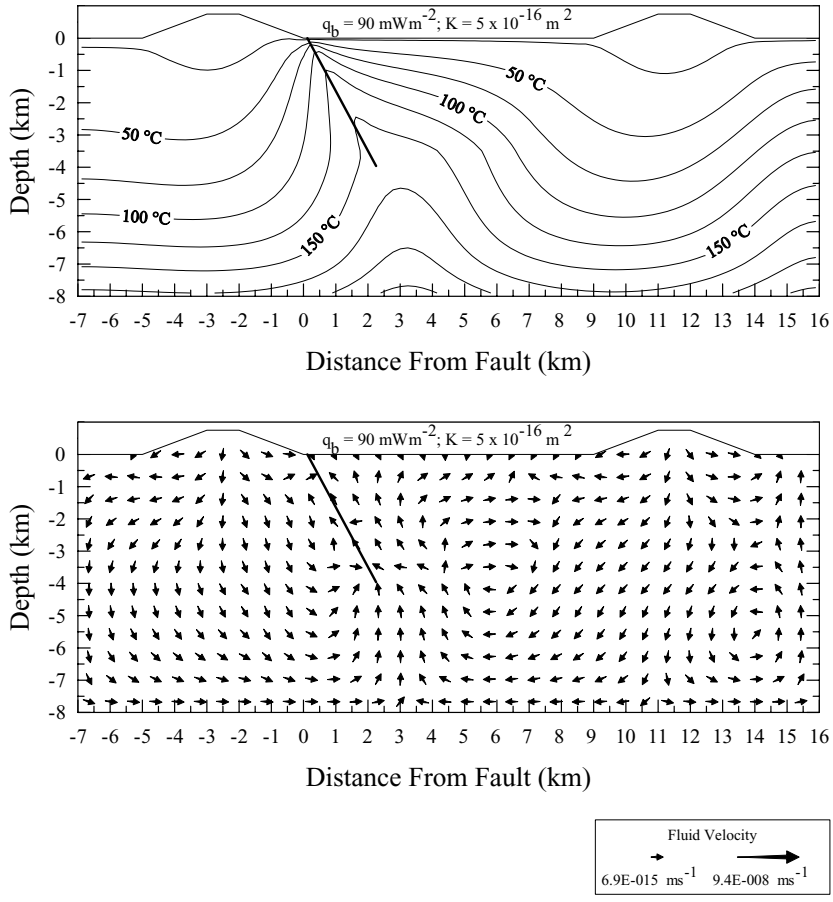

Fig. 7. Steady-state thermal and flow regime obtained utilizing a bulk rock permeability of 5×10^{-16} m^2, and a basal heat flow of 90 mW m^{-2}.

In typical extensional geothermal systems the fault temperature at shallow depths (0–2 km) is significantly warmer than a purely conductive model at an identical depth. However, with significant upflow, the expected higher fault temperatures may by "washed out" and actually be cooler than predicted by a conductive model. The very cool temperatures obtained from the steady-state 5×10^{-16} m^2 bulk rock permeability model (with respect to precision temperature measurements) suggest that transient effects may be important.

3. Transient results

Geothermal systems may require periodic earthquakes to prevent self-sealing of the permeable fault; hence the maximum fault temperature should reflect the recurrence interval on the fault. Typical Basin and Range faults appear to sustain large earthquakes every

1–20 kyear. The southern Dixie Valley fault last ruptured in 1954, but the area where the geothermal system is located has not ruptured for several thousand years (Caskey, personal communication, 2002). The problem of reconciling higher observed reservoir temperatures (from precision temperature logs) with the lower temperatures modeled at steady-state thus becomes the problem of determining where in the temporal evolution of the geothermal system production is situated. Hence, we next assess the effects of transient heating and cooling in the models developed above.

3.1. Fault temperature

Fig. 8a and b is the temperature–time histories for a cell located at the downdip edge of the fault, approximately 3.85 km below and 2.15 km to the right of the fault/valley contact (see Fig. 2), utilizing several bulk rock permeabilities and initial conditions. This particular cell

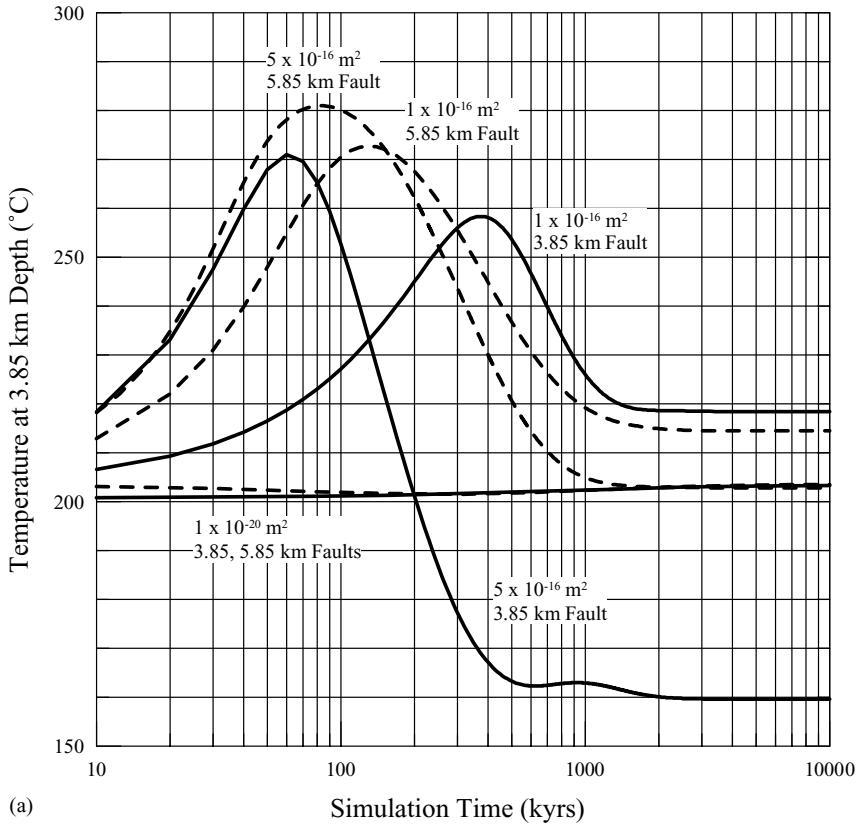

Fig. 8. (a) Temperature–time history of a cell at 3.86 km depth (solid lines for a 3.85 km deep fault, dotted lines for 5.85 km deep fault) for several bulk rock permeabilities utilizing a conductive thermal regime as the initial condition. (b) Temperature–time history of a cell at the base of the fault (3.85 km depth) for several bulk rock permeabilities utilizing a naturally-convective medium as the initial condition.

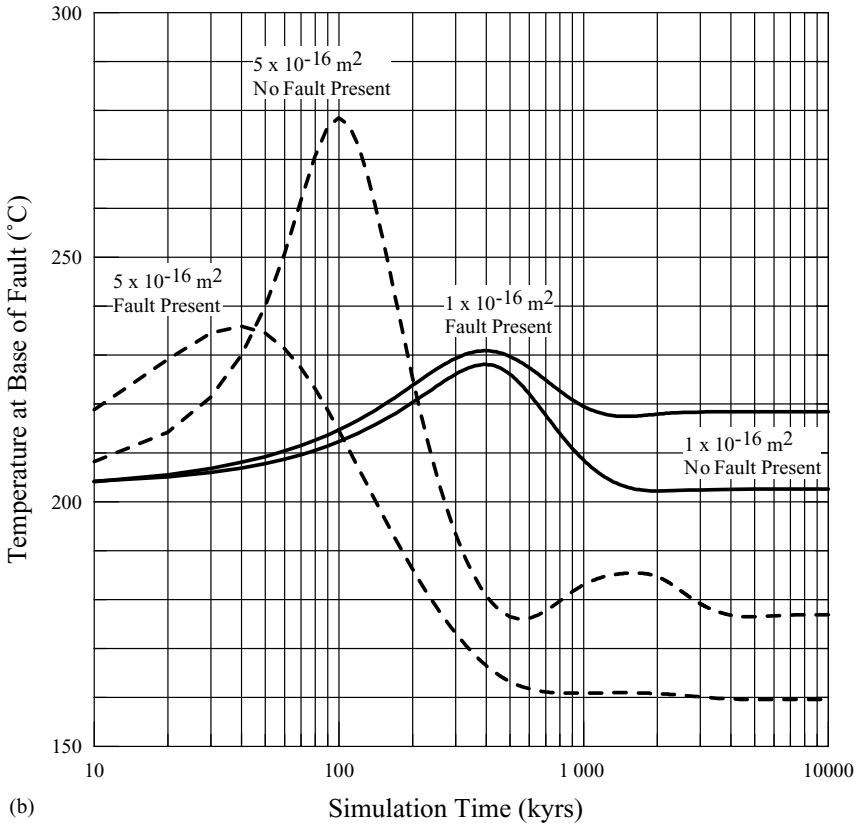

Fig. 8. (*Continued*).

essentially records the maximum fault modeled temperature. For models utilizing bulk rock permeabilities of 1×10^{-17} m^2 or below, the thermal regime is essentially conductive, and the temperature quickly reaches steady-state with only a few degrees of heating. For the higher bulk rock permeabilities, however, the temperature at the base of the fault varies strongly as a function of time. The maximum temperature for the cases where the starting regime is conductive is 255–275 °C. The temperature maximum does not occur at steady-state, but rather, within the first 60 kyear for the 5×10^{-16} m^2 bulk rock permeability model, and 359 kyear for the 1×10^{-16} m^2 bulk rock permeability model. Similar timing is observed for models that utilize freely convecting (i.e., no fault) porous media as initial conditions. However, for these models (e.g., Fig. 8b), the magnitude of the transient heating pulse is small and positive (1×10^{-16} m^2 bulk rock permeability) or larger and negative (5×10^{-16} m^2 bulk rock permeability). The transient behavior of these two models is a consequence of utilizing a fault-free convecting medium as initial conditions (e.g., Fig. 3b and c). The higher bulk rock permeability case is initially much hotter near the location of the future fault because the permeability contrast is greatest there. Hence, the fluid flow is focused along the left (due to the slight asymmetry in the model geometry) valley fill/bulk rock

contact even prior to the development of a fault. For the lower permeability case, there is no such contrast and the upflow is very symmetric about the midpoint of the model domain.

In all the simulations discussed above, the time step was at least 2.5 kyear for times <1 Myear. Other models utilizing a much smaller time step yield nearly identical results; hence, we believe that the time step of 0.6–2.5 kyear used by our simulations at times <1 Myear is sufficient to resolve the transient behavior of these systems. Furthermore, it appears that, much like actual geothermal systems, the models presented here "mine" heat over time, causing the system to cool significantly. Thus, the large difference between the steady-state temperatures predicted by the 1×10^{-16} and 5×10^{-16} m^2 models can be explained by the secondary convection present beneath the ranges in the one model, mining not only more heat, but at a faster rate. So much so, that the overall thermal regime is cooler. The secondary convection that develops as the system evolves may, however, be influenced by the model geometry. Future work will expand the distance between the ranges, as well as deepening the model to >10 km depth to investigate this effect.

Although the transient behavior described above may help explain the lower than measured predicted temperatures (both bulk rock permeability models predict temperatures that are lower than the ∼280 °C temperatures measured via precision temperature logs in Dixie Valley), several models with a 2 km deeper fault and valley fill sequence were investigated to address whether or not a deeper fault would resolve the discrepancy. Fig. 8a also shows the results from these models. Again, each temperature–time history is well resolved; however the maximum temperature for the lower bulk rock permeability case occurs about 200 kyear earlier, whereas the maximum temperature for the higher bulk rock permeability case occurs about 20 kyear later. The increase in fault temperature is only about 10–15 °C, which, albeit a small increase, is sufficient to match the measured temperature.

3.2. Surface heat flow

The predicted surface heat flow for the models at the simulation time corresponding to the maximum fault temperature for three different bulk rock permeability models (1×10^{-20}, 1×10^{-16}, and 5×10^{-16} m^2) is shown in Fig. 5a and b (note the scale change on the heat flow axis between the two panels). Because the maximum fault temperature for the conductive and no-fault convective initial conditions cases occurs at steady-state, the predicted heat flow does not change. However, the predicted heat flow at the fault/valley contact is almost 200 mW m^{-2} (1×10^{-16} m^2 case) and 500 mW m^{-2} (5×10^{-16} m^2 case) higher than for the respective steady-state cases. Furthermore, the predicted range of heat flow is somewhat higher due to the lower recharge rates at the earlier simulation times. Note also that the double peak in the predicted heat flow near the fault/valley contact for the (5×10^{-16} m^2 bulk rock permeability case) is an artifact of the rectangular grid used to discretize the model domain and is therefore not meaningful. A similar increase in predicted heat flow is also observed for the models that utilize a no-fault convecting medium as initial conditions: the transient heat flow increase for the 1×10^{-16} m^2 case is about 50 mW m^{-2}, but about 370 mW m^{-2} for the 1×10^{-16} m^2 case, again as a consequence of the initial flow geometry focusing more fluid near the future fault because of a slight asymmetry in the valley fill.

Wisian et al. (2001) calculated a heat loss of 1×10^7 W for the Dixie Valley geothermal system. The heat loss suggested by the predicted surface heat and mass flows obtained from our transient models is of the same order of magnitude. Thus, the class of models discussed should be good approximations of actual Basin and Range geothermal systems.

4. Conclusions

The most important observations obtained from our simulations are that temperatures in Basin and Range geothermal systems are highly time-dependent and the geologic history can dramatically modify the maximum reservoir temperature and the time-frame of occurrence. For example, the maximum fault temperature of about 245–275 °C obtained utilizing a bulk rock permeability of 5×10^{-16} m^2 does not occur at steady-state, but rather at 50–60 kyear, and is about 110–160 °C hotter than at steady-state. The 1×10^{-16} m^2 bulk rock permeability model behaves in a similar way. It is interesting to note that the temperature is not a function of the fault (high permeability) extent. A fault extending 2 km deeper than in the standard model yields similar behavior and temperatures. The modeling shows that the high temperatures needed to match the observed fault temperature, flow rates, and heat flow do require a regional permeability that allows significant flow to persist to depths of 6 km or more. This result suggests that the best initial conditions for high-temperature system development are an actively convecting porous medium, and not an essentially conductive thermal regime. We are currently studying thermal data from Basin and Range deep oil and geothermal wells to better understand the background, deep, thermal conditions. However, deeper drilling in the ranges adjacent to active geothermal systems may help identify the appropriate regime for modeling.

The complicated flow regimes modeled suggest that the heat present in the system is naturally "mined" over time causing the system to cool significantly; nonetheless, the system may persist for millions of years at commercially exploitable temperatures, especially for binary systems (∼150 °C). Hence, the problem of reconciling higher observed reservoir temperatures with the lower temperatures modeled at steady-state becomes the problem of determining where in the temporal-evolution history the geothermal system production is situated. If higher temperatures are observed, the implication from the models is that the present thermal and flow regime is early in the system's cycle. In fact, the present-day temperature and heat loss from the Dixie Valley geothermal system suggests that the system is not at steady-state, but rather somewhat earlier in the temporal evolution, perhaps only a few hundred thousand years. However, because both sets of initial conditions will generate the maximum thermal pulse very early in the life of the system (50–60 kyear), further work must be performed correlating the timing of Basin and Range faulting and geothermal systems before a preferred set of initial conditions is adopted.

The relatively high reservoir temperatures observed in some extensional geothermal systems (>280 °C) must be a function of oscillating high/low fault permeability maintained by seismicity along the range-bounding fault. Thus, the geothermal fluid is never truly depleted: the upflow simply wanes (or is rerouted) with decreasing fault permeability.

The location of hot springs and young faults in Nevada is shown in Fig. 9. Exploration drilling has been heavily concentrated along the area of the youngest faults in west-central

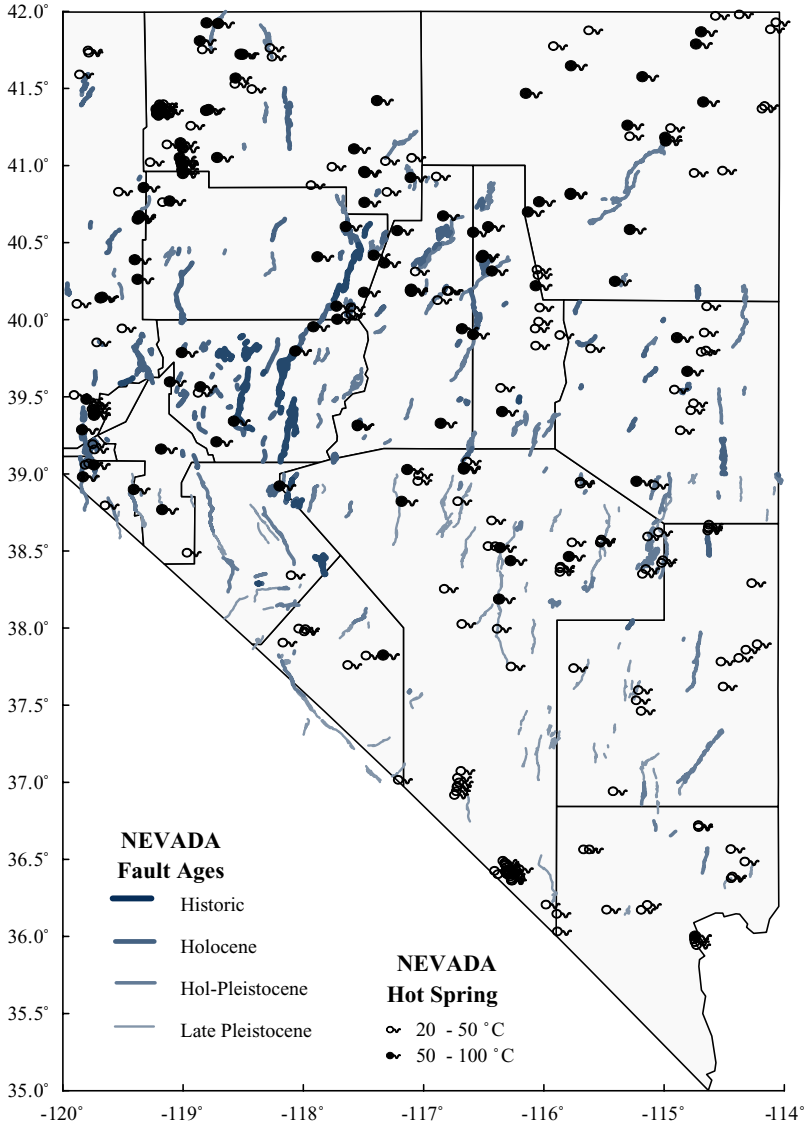

Fig. 9. High-temperature gradients, thermal springs, and faulting in Nevada.

Nevada (Richards and Blackwell, 2002). Associations of hottest geothermal systems have been made with the young northeast-trending faults (see Coolbaugh et al., 2002). All faults that are late Pleistocene and younger from the recent USGS compilation of faulting (Quaternary faults and fold database of the United States, 2003) are shown in Fig. 9. Most of the hot springs with temperatures greater than 50 °C are associated with these faults, with the exception of the extreme northwest part of Nevada (Black Rock Desert, north to

Baltazor Hot Springs on the Oregon border) and the northeast part of Nevada. On the other hand, some of the young faults seem to have no hot springs at all and in the eastern part of the state there are fewer high-temperature springs. Lower crustal temperatures because of the presence of extensive carbonate aquifers (Lachenbruch and Sass, 1978) is the conventional explanation. The modeling results discussed above, however, suggest that this area should be re-examined to verify whether this is a real effect or there is masking of the hotter systems by the carbonate aquifer flow at shallow depths. Geologically, these areas also seem attractive for geothermal exploration. Regional clusters of warm springs in several places might be related to flow in the local absence of high-permeability fault conduits, such as can be seen in the no-fault models shown in Fig. 3b and c.

Acknowledgements

This work was supported by D.O.E. Contract DE-FG07-02ID14414. The authors wish to acknowledge Ken Wisian for his help in setting up the models, and Stefan Finsterle and Karsten Pruess for their assistance with TOUGH2. A detailed review by Sabodh Garg greatly improved the clarity of the manuscript.

References

Benoit, W.R., 1999. Conceptual models of the Dixie Valley, Nevada, geothermal system. Geotherm. Resour. Council Trans. 23, 505–511.

Blackwell, D.D., 1983. Heat flow in the Northern Basin and Range province. In: The role of heat in the development of energy and mineral resources in the Northern Basin and Range province. Geothermal Resources Council Special Report, vol. 13. pp. 81–92.

Blackwell, D.D., Steele, J.L., Carter, L.S., 1991. Heat flow patterns of the North American Continent: a discussion of the DNAG geothermal map of North America. In: Slemmons, D.B., Engdahl, E.R., Zoback, M.D., Blackwell, D.D. (Eds.), Neotectonics of North America. Geological Society of America, pp. 423–436.

Blackwell, D.D., Gollan, B., Benoit, D., 2000. Temperatures in the Dixie Valley, Nevada, geothermal system. Geotherm. Resour. Council Trans. 24, 223–228.

Blackwell, D.D., Leidig, M., Smith, R.P., 2002. Regional geophysics of the Dixie Valley area: example of a large Basin and Range geothermal system. Geotherm. Resour. Council Trans. 26, 519–523.

Blackwell, D.D., Benoit, D., Golan, B., Wisian, K.W., 1999. Structure of the Dixie Valley geothermal system, a "typical" Basin and Range geothermal system. Geotherm. Resour. Council Trans. 23, 525–531.

Brikowski, T.H., 2001. Modeling supercritical systems with TOUGH2: The EOS1sc equation of state module and a Basin and Range example. Geotherm. Resour. Council Trans. 25, 285–290.

Caskey, S.J., Bell, J.W., Slemmons, D.B., Ramelli, A.R., 2000. Historical surface faulting and paleoseismology of the central Nevada seismic belt. In: Lageson, D.R., Peters, S.G., Lahren, M.M. (Eds.), Great Basin and Sierra Nevada: Boulder, Colorado, Geological Society of America Field Trip Guide, vol. 2. pp. 23–44.

Coolbaugh, M.F., Taranik, J.V., Raines, G.L., Shevenell, L.A., Sawatzky, D.L., Bedell, R., Minor, T.B., 2002. A geothermal GIS for Nevada: defining regional controls and favorable exploration terrains for extensional geothermal systems. Geotherm. Resour. Council Trans. 26, 485–490.

Kennedy, B.M., Fischer, T.P., Shuster, D.L., 2000. Heat and helium in geothermal systems. In: Proceedings of the Twenty-fifth Workshop on Geothermal Reservoir Engineering. Stanford Geothermal Program Report SGP-TR-165, pp. 167–173.

Ingebritsen, S.E., 1999. Geological implications of a permeability-depth curve for the continental crust. Geology 27, 1107–1110.

Lachenbruch, A.H., Sass, J.H. 1978. Models of an extending lithosphere and heat flow in the Basin and Range province. In: Smith, R.B., Eaton, G.P. (Eds.), Cenozoic Tectonics and Regional Geophysics of the Western Cordillera. Geological Society of America Memoir, vol. 152. pp. 209–250.

Parry, W.T., Hedderly-Smith, D., Bruhn, R.L., 1991. Fluid inclusions and hydrothermal alteration on the Dixie Valley fault, Nevada. J. Geophys. Res. 96, 19733–19748.

Pruess, K., Oldenburg, C., Moridis, G., 1999. TOUGH2 User's Guide, Version 2.0. Report LBNL-43134, Lawrence Berkeley National Laboratory, Berkeley, CA, 197 pp.

Quaternary faults and fold database of the United States, 2003. US Geological Survey, Version 1, http://qfaults.cr.usgs.gov/faults.

Richards, M., Blackwell, D.D., 2002. The forgotten ones: geothermal roads less traveled in Nevada. Geotherm. Resour. Council Bull. 31, 69–75.

Wisian, K.W., Blackwell, D.D., Richards, M., 2001. Correlation of surface heat loss and total energy production for geothermal systems. Geotherm. Resour. Council Trans. 25, 331–336.

Wisian, K.W., 2000. Insights into extensional geothermal systems from numerical modeling. In: Proceedings of the World Geothermal Congress 2000, vol. 3. pp. 1947–1952.